International Journal of Environmental Science and Technology (2022) 19:6099–6116
https://doi.org/10.1007/s13762-021-03787-0

ORIGINAL PAPER

Performance evaluation of enhanced geothermal-based desiccant cooling and heating systems for an office building

A. Hassanpour[1] · M. Borji[1] · B. M. Ziapour[2]

Received: 2 March 2021 / Revised: 26 August 2021 / Accepted: 2 November 2021 / Published online: 28 January 2022
© Islamic Azad University (IAU) 2021

Abstract

In the present study, two new geothermal energy-driven configurations of a solid desiccant air cooling system integrated with an air handling unit for space cooling and heating of a case office are proposed. The geothermal energy is extracted by the thermosiphon pipes and delivered to a two-level cascade heat exchanger. The first thermal level supports the regeneration demand of cooling system, and the heating unit receives its thermal demand from the second thermal level of the heat exchanger. The parametric study is performed to analyze the effect of the various operating parameters on the system's efficiency. The appropriate parameters, such as the temperature of regenerated air, the supplied air's mass flow rate, humidity ratio, and ambient temperature, are considered. Also, the performance of the cycle is analyzed from energy and exergy point of view according to the cooling and heating loads of the considered office building. So, the obtained results indicate that energy efficiency for the desiccant evaporative recirculation and desiccant evaporative ventilation systems is about 81.75% and 81.8%, respectively. The exergy efficiency for desiccant evaporative recirculation in the heating and cooling systems is about 50.2% and 5.42%, respectively, and these values for the desiccant evaporative ventilation system are about 34.8% and 11.6%, respectively.

Keywords Desiccant air cooling system · Air handling unit · Thermosiphon pipe · Geothermal energy · Office building

List of Symbols

A_{out}	External surface area of thermosiphon (m^2)
A_{in}	Internal surface area of thermosiphon (m^2)
COP	Coefficient of performance
COP_C	Carnot COP
COP_{rev}	Reversible COP
$COP_{R,C}$	COP of a Carnot refrigerator
$\dot{E}_{cooling}$	Exergy rate of cooling capacity
$\dot{E}_{lost}$	Rate of exergy destruction (kW)
$\dot{E}_{lost,Total}$	Exergy destruction for the whole desiccant system (kW)
$\dot{E}_{reg}$	Regeneration exergy rate (kW)
h	Enthalpy of moist air (kJ/kgdryair)
$h_{e,c}$	Convection heat transfer coefficients ($kW/m^2.K$)
h_{fg}	Enthalpy of vaporization of water (kJ/kg)
H_L	Latent heat of vaporization of heat pipe working fluid (J/kg)
K	Thermal conductivity (W/m.K)
$L_{e,c}$	Heat pipe length (m)
$\dot{m}_a$	Mass flow rate of air (kg/s)
$\dot{m}_{w1}$	Humidity added to EC_i (kg/s)
P_v	Vapor pressure of heat pipe working fluid (Pa)
$\dot{Q}_{AHU}$	Required thermal energy of the building (kW)
$\dot{Q}_{Cooling}$	Ratio of the Cooling load of space (kW)
$\dot{Q}_{Heating}$	Ratio of the Heatig load of space (kW)
$\dot{Q}_{Reg}$	Requirement heat of regeneration section (kW)
W_{out}	Work output from Carnot heat engine
q_{TP}	Heat transfer from the thermosiphon pipe (kW)
R	Thermal resistivity
R_{in}	Internal heat pipe radius (m)
R_{out}	External heat pipe radius (m)
R_w	Heat pipe wick internal radius (m)
s	Entropy of moist air

Editorial responsibility: Samareh Mirkia.

✉ M. Borji
mborji@liau.ac.ir

1 Department of Mechanical Engineering, Islamic Azad University, Lahijan Branch, Lahijan, Iran

2 Department of Mechanical Engineering, University of Mohaghegh Ardabili, Ardabil, Iran

$\dot{S}_{gen}$	Entropy generation (kJ/K)
s_w	Entropy of liquid water (kJ/K.kgdryair)
T	Temperature (K)
$T_{ambient}$	Ambient temperature (K)
T_e	Carnot equivalent temperature of evaporator (K)
T_i	Dry-bulb temperature (K)
T_s	Carnot equivalent temperature of heat source (K)
T_{source}	Heat source temperatures (K)
T_{space}	Space temperatures (K)
T_{wb}	Wet-bulb temperature (°C)

Acronyms

AHU	Air Handling Unit
CL − GCT	Closed-Loop GCT
DCS	Desiccant Air cooling System
DER	Desiccant Evaporative Recirculation
DEV	Desiccant Evaporative Ventilation
DW	Desiccant Wheel
EC	Evaporative Cooler
RR	Rotary Regenerator
GCT	Ground Coupled Thermosiphon
GSHE	Ground Sorce Heat Exchanger
RH	Relative Humidity
HE	Heat Exchanger
ST − GCT	Single-Tube GCT
$\dot{Q}_{Source}$	Thermal energy from the geothermal (kW)

Greek Symbols

ω	$\omega_2 = 0\omega_2 = 0$ Specific humidity or humidity ratio (kgwater/kgdryair)
ε	Effectiveness
$\eta_{th,c}$	Thermal efficiency of Carnot heat engine
$\eta_{II,total}$	Total exergy destruction of the proposed cycle
$\eta_{I,total}$	Total energy efficiency of the proposed cycle

Introduction

Thermal comfort needs conditioning the outdoor air to control the dry-bulb temperature and moisture content (Thu et al. 2018). The air temperature and its humidity should be controlled directly, especially for the hot and humid areas. As a conventional air conditioner system (Thu et al. 2018), the vapor compression air-conditioning system cools down air temperature to its dew point temperature and then reheated to the proper temperature; this process requires significant energy consumption. Recently, many pieces of research were done about desiccant dehumidification systems. Desiccants can remove the air humidity due to the vapor pressure between the air and desiccants. The desiccants can be regenerated by solar energy and other waste energy resources (Chen et al. 2018; Gómez-Castro et al. 2018; Kabeel et al. 2018a). The desiccant dehumidification systems are environmentally friendly compared to the condensation ones (Thu et al. 2018; Xie et al. 2016; Yinglin et al. 2016). Hence, the desiccant dehumidification systems are extensively used in different areas like water production, ventilation, and cultivation (Ali et al. 2017; Chang et al. 2018; William et al. 2015). Generally, there are two types of desiccant cooling systems, including liquid and solid. The liquid desiccant cooling system contains a regenerator and absorber. The solid one has a solid rotary desiccant, heat exchanger, and regenerator. A liquid desiccant dehumidification system was designed by (Ali et al. 2017) to provide the required relative humidity of a greenhouse. Another study was performed by (William et al. 2015), based on a desiccant air cooling system to improve freshwater production and storage issues. The use of desiccant wheels as an air conditioning system with the advantages of low energy consumption was investigated by (Chang et al. 2018).

The liquid desiccants have significant benefits compared to the solid desiccant systems, such as lower temperature for regeneration, higher capacity of absorption, and lower pressure drops (Chen et al. 2018; Mohammad et al. 2013). Recently, several research studies have been reported on the development of liquid desiccant systems spanning from theoretical analyses to experiments. To enhance efficiency of desiccants, (Yang et al. 2015, 2014) experimentally used ultrasonic atomization system for increasing the contact area between the air and desiccant solution to improve the dehumidification performance. (Kabeel 2010) experimentally investigated the liquid desiccant system efficiency in humidification–dehumidification (HDH) processes by the injection of air to the desiccant solution. The results showed that the system effectiveness in dehumidification and humidification processes was about 0.87 and 0.92, respectively. A liquid desiccant with an evaporative cooler was devised by (Chen et al. 2018) for the treatment of fresh air. The humid and hot fresh air was dehumidified by the desiccant wheel and then direct evaporative cooler sensibly cooled down the air. Compared to the traditional air conditioning system, the power consumption of this system was about 22.4–53.2% lower. Also, (Kabeel et al. 2018b) presented two dynamic models comprising transient and discrete steady-state models. Their proposed air cooling system was regenerated by solar thermal energy. The error between the simulation model and the experimental result was less than 4%. The effect of the falling liquid desiccant flow on the finned tubes for cooling and dehumidifying air was analyzed by (Nada 2017). Various desiccant flow classification was simulated numerically, and obtained data declared that the parallel flow arrangement had better efficiency for cooling and dehumidifying. A mathematical model extracted from the finite difference method by considering heat and mass transfer is

developed by (Emhofer et al. 2017). The effect of geometric variables on the dehumidifier performance of desiccant for finding its best geometry was investigated. (Park et al. 2016) experimentally predicted the effectiveness of dehumidification in the liquid desiccant system. The effect of six operation parameters was considered. Based on the results, a good agreement with the system predicted efficiency was observed; the error between them was less than 10%.

Using renewable energy sources to drive the building cooling systems has some benefits like better control of inlet air quality, power saving, and reduction in CO_2 emission compared to conventional air cooling systems (Fong and Lee 2020). Renewable energy-based cooling systems are also economical due to their thermal energy resources (Caliskan et al. 2019). Renewable energy supports the regeneration process of the desiccant wheels to dehumidify the air. The air is regenerated and cooled down sensibly in the heat regenerator and delivered to the indirect evaporative cooler (Bourdoukan et al. 2009). Shallow geothermal energy as clean energy is contained in the rocks and fluids beneath the ground. The most common way to extract the thermal energy from underground is based on the convection of heat-carrier fluid in buried plastic pipe loops, e.g., U-tubes or coaxial tubes, under the driving of circulation pumps (Wang et al. 2020).

The shallow geothermal energy can also be extracted by utilizing the gravity-assisted heat pipes, or referred to as thermosiphon, in which the heat is transferred based on vaporization and condensation and passive self-circulation of working fluid into the thermosiphon with a small temperature difference (Wang et al. 2017). With the thermosiphon based on shallow geothermal energy, no extra energy is required throughout the entire service life (Zorn et al. 2015). Apparently, the application of thermosiphons in geothermal utilization allows a lower maintenance cost and thus higher efficiency. There are two kinds of the ground-coupled thermosiphon (GCT) as the shallow geothermal energy system, including single-tube GCT (ST-GCT) and two-phase closed-loop GCT (CL-GCT) system (Hassanpour et al. 2020).

Efficient cooling and heating techniques have been proposed based on shallow geothermal energy resource. A solar and shallow geothermal-based air cooling system was designed by (Rosiek and Batlles 2012). Geothermal energy was applied as an alternative system to provide the required energy of the cooling tower of the absorption chiller with a temperature of 22°C. The results showed 31% less electrical energy consumption, and also the proposed system could save 116m^3 water consumption during the summer. An improved circulating fluidized bed dehumidification system integrated with geothermal and solar thermal energies is proposed by (Liang et al. 2018). In their systems, the shallow geothermal energy was used to precool the air and increase the relative humidity. According to the results, dehumidification performance of the system was significantly improved. By employing borehole heat exchangers, a ground-coupled desiccant air conditioning system was presented by (Speerforck et al. 2017; Speerforck and Schmitz 2016). Desiccant wheel and a heat recovery wheel precooled and dehumidified outdoor air. Based on the reported data, using geothermal energy resources entails 70% energy saving compared to traditional air conditioning systems. (Rayegan et al. 2020) performed a transient modeling and multi-objective optimization of a solar-assisted desiccant cooling system integrated with ground source renewable energy. Their results revealed that, without a ground source heat exchanger, the system cannot afford thermal comfort in highly humid regions even with high regeneration temperatures. (Liang et al. 2020) experimentally analyzed a liquid desiccant dehumidification system combined with shallow geothermal energy. According to the obtained results, considering similar working conditions, their devised plant could save 86% and 82% power in comparison with the condensation system and the traditional liquid desiccant dehumidification system, respectively. (Berardi et al. 2020) analyzed the hourly operation of the Uçkan configuration of the desiccant system that uses combined ground and solar energies. They showed that the payback period varies in 5−7years without and with GSHE before and after DW.

Main contributions and novelties

The building construction divisions hold one-third of global energy consumption and approximately 40% of total direct and indirect CO_2 emissions. Also, around 50% of the energy consumed in buildings is for air conditioning purposes. In extremely hot and humid areas, about 80% of the needed energy is consumed in cooling systems (Heidari et al. 2019). Accordingly, the use of renewable energy sources has been widely attracted in different areas. Among various green and renewable energy resources, geothermal energy attracted great attention due to its vast worldwide sources and non-intermittent nature.

In the present study, two novel heating and cooling systems based on shallow geothermal energy sources are devised for a case office building located in Sarein, Ardabil, Iran. Sarein city is a promising area for geothermal energy with a multitude of thermal springs with a temperature of 80–100 °C (Yousefi et al. 2010). The extraction of thermal energy from the geothermal wells is performed using two-phase closed-loop ground-coupled thermosiphons (CL-GCTs). The CL-GCT system extracts the geothermal energy to regenerate the desiccant air conditioning system and provide the energy demand of Air handling unit (AHU). The effect of design parameters, including ambient temperature, regeneration temperature of desiccant, and air mass flow rate on the system thermal and electrical

efficiencies, are investigated. Also, the proposed building energy and optimum diameter of the CL-GCT system to supply the building required energy are analyzed, and the energy and exergy analyses are conducted for all components of the system.

Materials and methods

The proposed system includes two main parts: the thermal energy extraction part from underground by CL-GCT system and energy conversion section by desiccant air conditioning system and AHU to support the heating and cooling demands of an office building in the Sarein city, Ardabil, Iran. The delivered thermal energy to the cascade heat exchanger is supported by the two-phase closed-loop ground-coupled thermosiphon with a length of 150m and a spring temperature of 85°C. The schematic diagram of the proposed systems is shown in Fig. 1. The cascade heat exchanger has two energy levels; so, the outlet flow of the CL-CGT (state 14) exchanges its heat with two subsystems in the cascade heat exchanger (process 14 → 15, and process 15 → 16) and is delivered into the reservoir (state 16). Finally, it flows back to the hot thermosyphon (state 12).

The desiccant air conditioning system is applied to supply the cooling demands of the considered office building. Two different desiccant air cooling systems are designed: (1) Desiccant Evaporative Ventilation cycle (DEV) and (2) Desiccant Evaporative Recirculation cycle (DER). In the DEV system, the ambient air before entering the evaporative cooler mixes with the conditioned air of the building (states 0 and 1) that is illustrated in Fig. 1a. For the DER system, the ambient air before entering the desiccant wheel mixes with the conditioned air of the building (states 0 and 1) as shown in Fig. 1b. Besides, two main lines, including the regeneration channel (upper channel) and supplied channel (lower channel), can be introduced for desiccant air cooling systems. In the regeneration channel, for absorbing humidity by the desiccant wheel (process 8 → 9), the air is heated in the heat exchanger (process 7 → 8) by the hot water coming from the CL-GCT system. In the regeneration channel, the inlet air at state 5 flows through the evaporative cooler 2 (state 6) and cools down to its dew point temperature. Then, the air is heated in the rotary air-to-air heat exchanger. The desiccant wheel absorbs the air humidity in process 8 → 9 and deliveries it to the inlet air in process 1 → 2; so, the air humidity in state 2 increases. The humid air in state 2 flows through the rotary air-to-air heat exchanger and is cooled down with a constant humidity ratio. Finally, the air is entered into the evaporative cooler 1 to reach the considered temperature and humidity for building cooling (state 4). Besides, to supply the heating demand of the building, an AHU system is applied. The required energy of the AHU system is provided in process 18 → 19.

A similar description can be presented for the desiccant evaporative recirculation cycle, the only difference is that in the DER system; the ambient air before entering the desiccant wheel mixes with the conditioned air of the building.

Case study building characteristics

As mentioned earlier, Sarein city in Ardabil, Iran, is chosen due to its hot water springs with a temperature of up to 45 °C. The existence of different hot water springs is because of the inactive volcanic Sabalan Mountain.

In this study, a ten-story office building is selected. The office building is located in Sarein, Ardabil, Iran, which has a geographical coordinate of latitude: 38°08′60.00εN and longitude: 48°03′60.00εE. The outdoor design temperatures for the winter and summer are -21.9°C and 29.7°C, respectively. This building has ten floors with a total area of 4808m^2 with an average area of 480m^2 for each floor with useful office space of 410m^2 including various office spaces, such as technical experts room, presidency room, conference room, computer server room, pantry, and bathroom. According to NEN 1824:2010 NL standard, the minimum requirement for space in an office building is 7m^2. Therefore, considering useful office space for each zone, the air conditioning calculations were evaluated for 58 people. The building's heating and cooling load are calculated using the Hourly Analysis Program V4.9 (HAP) based on the building information tabulated in Table 1. The plan of the considered building is demonstrated in Fig. 2.

The cooling and heating loads of the each story of the building to design the proposed system for supporting the demands are calculated approximately 206 and 447kW, respectively.

Mathematical modeling

The proposed system is devised to provide cooling and heating of an office building. The simulation is carried out in the EES software. In order to evaluate the efficiency of the proposed system, energy and exergy analyses are conducted.

Two-phase closed-loop system

The proposed thermosiphon pipe is simulated to calculate the optimum diameter. The thermal resistances of the thermosiphon are shown in Fig. 3.

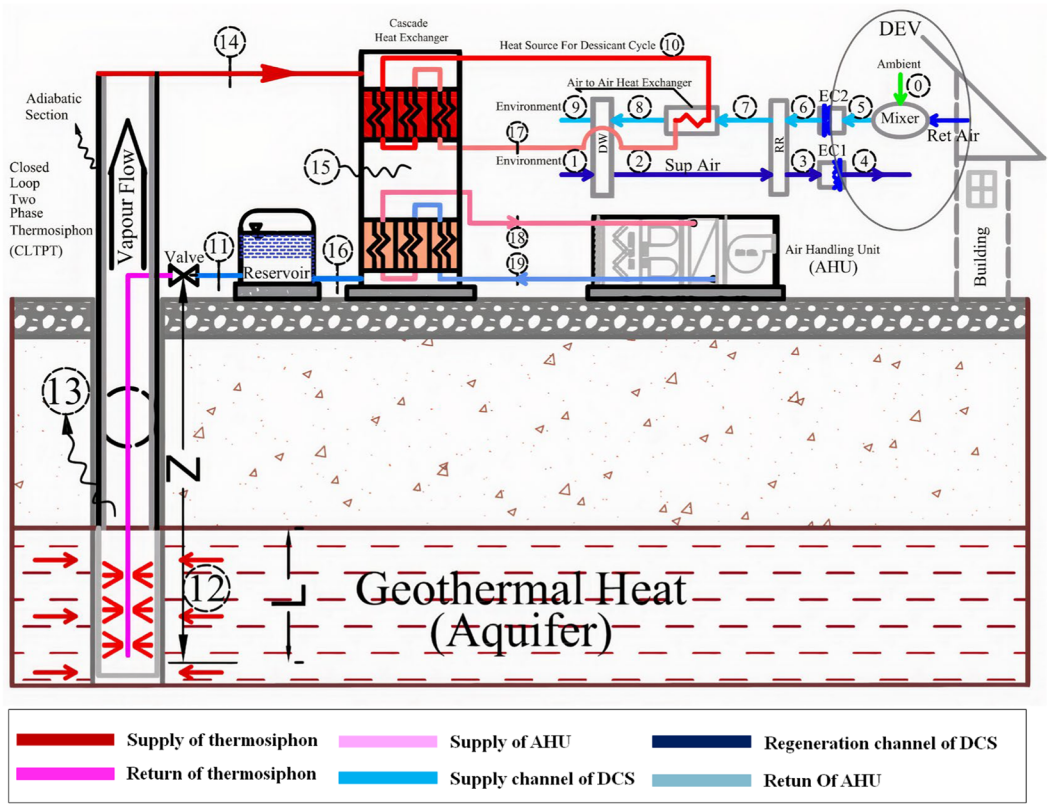

(a)

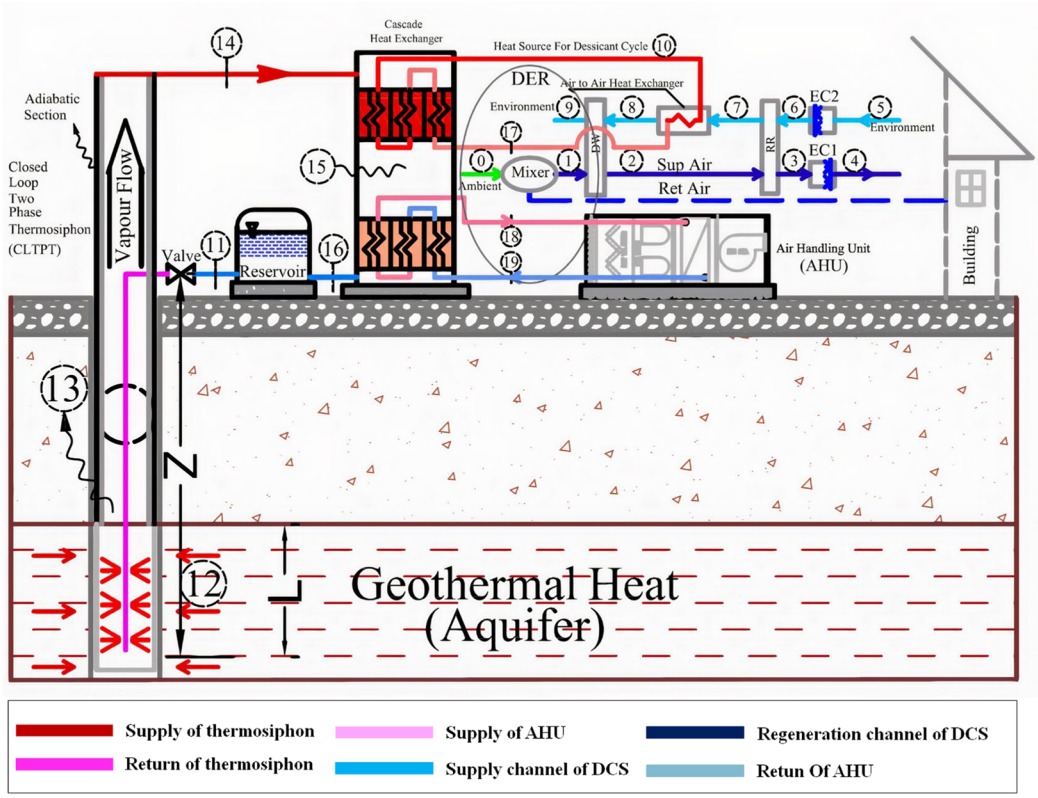

(b)

Fig. 1 Configurations of proposed cooling systems; **a** DEV system and **b** DER system

Table 1 Building characterization

Parameters	Value
Total area of building	4808m^2
Activity	Office
Glazing Type	Double glazing (Two panes of 3mm thick clear glass with a 13mm air gap)
Story Number	10
Total heating load	447kW
Total cooling load	206kW

Based on Fig. 3, there are nine thermal resistances for each heat pipe, and the water is the working fluid of the CL-GCT system. For condenser and evaporator sections, the external thermal resistance can be presented as:

$$R_{1,9} = \frac{1}{2h_{e,c} \cdot A_{out}} \tag{1}$$

where $h_{e,c}$ indicates the sum of radiation and convection heat transfer coefficients for a surface that is immersed in the fluidized bed and is equal to 300W/m^{2}K (Mojaver et al. 2018). A_{out} is defined as the external surface of thermosiphon and can be defined by (Dunn and Reay 2016):

$$A_{out} = 2\pi \cdot R_{out} \cdot L_{e,c} \tag{2}$$

where L_e and L_c are the evaporator and condenser lengths, respectively. The conductive thermal resistance inside the thermosiphon is calculated by (Dunn and Reay 2016):

$$R_{2,8} = \frac{\ln\left(R_{out}/R_{in}\right)}{2\pi \cdot K_m \cdot L_{e,c}} \tag{3}$$

where K_m is the thermal conduction of the cell. R_3 and R_7 stand for the wick of the thermosyphon as (Dunn and Reay 2016):

$$R_{3,7} = \frac{\ln\left(R_{in}/R_w\right)}{2\pi \cdot k_w \cdot L_{e,c}} \tag{4}$$

The wetted mesh wick thermal conduction is presented by K_w (Dunn and Reay 2016). R_4 and R_6 are the liquid and steam internal resistances, which are calculated by (Dunn and Reay 2016):

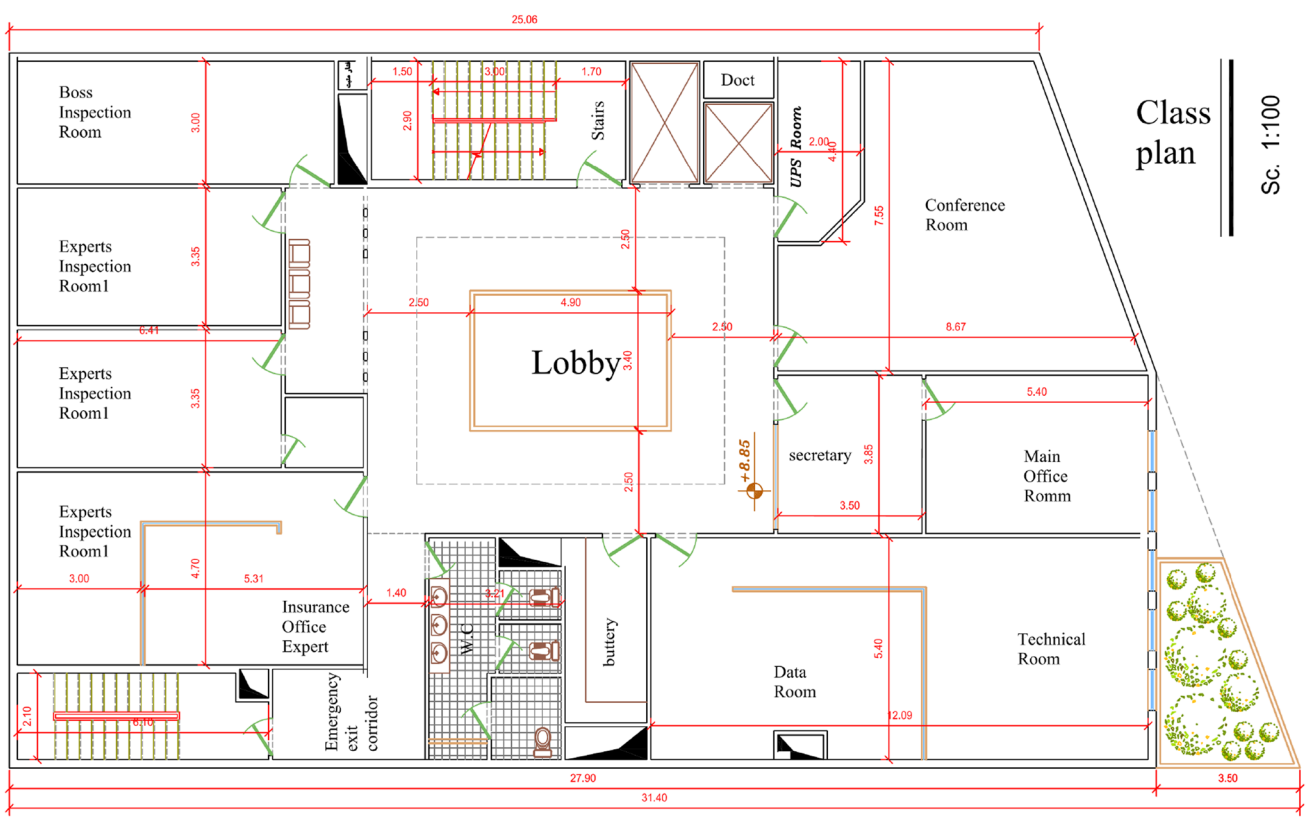

Fig. 2 The office building plan (All the lengths are in m)

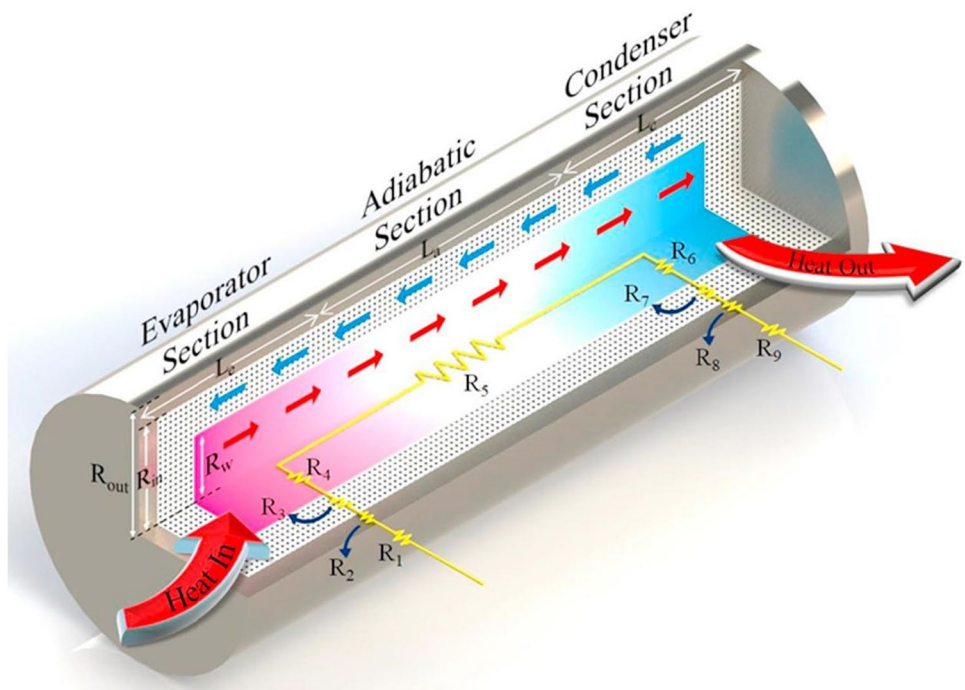

Fig. 3 Thermal model and operating principle of heat pipe

Table 2 Input parameters of thermosiphon

q_{TP}(kW)	T_{in}(°C)	T_{out}(°C)	L_e, L_c(m)	K_m(W/m.K)
68.5	85	80	1	27

$$R_{4,6} = \frac{\overline{R} \cdot T^2 \cdot \left(2\pi \cdot \overline{R} \cdot T\right)^{1/2}}{H_l^2 \cdot P_v \cdot A_{in}} \tag{5}$$

where H_l is the vaporization latent heat, P_v is the vapor pressure of heat pipe, and A_{in} is the surface of the liquid–vapor interface ($A_{in} = 2\pi.R_w.L_{e,c}$). R_5 is caused by the temperature drop in the steam transferred from condenser and evaporator, which can be neglected (Dunn and Reay 2016). The thermophysical characteristics of the thermosiphon are presented in Table 2 (Mills 1995).

The overall thermal resistance for the proposed thermosiphon can be written as (Mojaver et al. 2018):

$$R_{total} = \sum_{i=1}^{9} R_i \tag{6}$$

The heat transfer from the thermosiphon pipe can be calculated as follows (Mojaver et al. 2018):

$$q_{TP} = \frac{T_{in} - T_{out}}{R_{total}} \tag{7}$$

Based on the abovementioned equations, the optimum diameter for the thermosiphon pipe is computed.

The desiccant air conditioning system

Energy analysis of desiccant air cooling system

The proposed desiccant air conditioning system running in DER and DEV modes is illustrated in Fig. 1. In the ideal state, the desiccant wheel dehumidify the air completely; therefore, it can be concluded that (Kanoğlu et al. 2007);

$$\omega_2 = 0 \tag{8}$$

For the rotary regenerator, the maximum heat transfer occurs when the supplied channel air temperature at the outlet of the rotary regenerator cooled down to the regeneration channel flow temperature at the inlet of this component (Kanoğlu et al. 2007).

$$T_3 = T_6 \tag{9}$$

The air mass flow rate in two channels (supplied and regeneration) is equal. The energy balance can be written as follows for the rotary regenerator (Kanoğlu et al. 2007):

$$h_2 - h_3 = h_7 - h_6 \tag{10}$$

Also, specific humidity across the rotary regenerator for both supplied and regeneration channels stay constant (Kanoğlu et al. 2007):

$$\omega_2 = \omega_3 \tag{11}$$

$$\omega_7 = \omega_6 \tag{12}$$

Regarding that the mass flow rates are equal in supplied and regeneration lines, the effectiveness of the rotary regenerator is given by (Kanoğlu et al. 2004):

$$\varepsilon_{RR} = \frac{T_2 - T_3}{T_2 - T_6} \tag{13}$$

In the desiccant wheel with the ideal operation condition, the supplied heat from the geothermal energy to regeneration air must be no more than the latent heat required for the dehumidification of air in the desiccant wheel. So, the regeneration heat can be written as (Kanoğlu et al. 2004):

$$q_{reg} = (\omega_1 - \omega_2)h_{fg} = (\omega_9 - \omega_8)h_{fg} \tag{14}$$

where the latent heat of vaporization is presented by h_{fg}. Also, the energy balance of the adiabatic desiccant wheel can be written as (Kanoğlu et al. 2004):

$$q_{reg} = h_8 - h_9 = h_2 - h_1 \tag{15}$$

The effectiveness of the desiccant wheel can be written as:

$$\varepsilon_{DW} = \frac{T_2 - T_1}{T_8 - T_1} \tag{16}$$

Also, the another effectiveness relation for desiccant wheel can be defined according to the dehumidification efficiency of the wheel based on the input thermal energy of the regeneration channel, which can be calculated as follow (Kanoğlu et al. 2004):

$$\varepsilon_{DW} = \frac{(\omega_1 - \omega_2)h_{fg}}{h_8 - h_7} \tag{17}$$

In the evaporative cooler (EC), the humidification is an adiabatic process with constant wet-bulb temperature. For ideal case, the leaving air of the evaporative cooler has 100% humidity:

$$T_4 = T_{wb3} \tag{18}$$

$$RH_4 \cong 1 \tag{19}$$

The effectiveness of the evaporative coolers is (Kanoğlu et al. 2004):

$$\varepsilon_{EC} = \frac{T_{in} - T_{out}}{T_{in} - T_{wb,in}} \tag{20}$$

where T_{in} and T_{out} are dry-bulb temperatures of EC in its inlet and outlet, respectively. Also, $T_{wb,in}$ is the wet-bulb temperature of moist air at the entrance of EC. It is assumed that wet-bulb temperature is constant for the humidification process:

$$T_{wb,in} = T_{wb,out} \tag{21}$$

Therefore, for EC 1 and EC 2, the effectiveness can be written as follows (Kanoğlu et al. 2004):

$$\varepsilon_{EC1} = \frac{T_3 - T_4}{T_3 - T_{wb,3}} \tag{22}$$

$$\varepsilon_{EC2} = \frac{T_5 - T_6}{T_5 - T_{wb,5}} \tag{23}$$

The mass balances of evaporative coolers can be presented as (Kanoğlu et al. 2004):

$$\dot{m}_{w1} = \dot{m}_a(\omega_4 - \omega_3) \tag{24}$$

$$\dot{m}_{w2} = \dot{m}_a(\omega_6 - \omega_5) \tag{25}$$

where $\dot{m}_{w1}$ and $\dot{m}_{w2}$ denote the moisture rates that are added to air in the evaporative coolers in supplied and regeneration channels, respectively. The COP of the proposed air cooling system is defined as the ratio of the cooling load of space to the required heat of regeneration section. So, the coefficient of performance is calculated by (Kanoğlu et al. 2004):

$$COP = \frac{\dot{Q}_{Cooling}}{\dot{Q}_{reg}} \tag{26}$$

Besides, the total energy efficiency of the proposed cycle can be defined as:

$$\eta_{I,total} = \frac{\dot{Q}_{Cooling} + \dot{Q}_{Heating}}{\dot{Q}_{Source}} \tag{27}$$

Exergy analysis of desiccant and air handling unit

The maximum performance for the air cooling system can be obtained when the cycle is totally reversible. The cooling system would be reversible if the heat from the heat source were transferred to a Carnot heat engine, and the work output of this engine is supplied to a Carnot refrigerator to remove heat from the cooled space (Cengel et al. 2011). Therefore, the Carnot heat engine output work (W_{out}), refrigerator cooling load (q_L) and COP of the entire system can be expressed as follows:

$$W_{out} = \eta_{th,c} q_{in} \tag{28}$$

$$q_L = COP_{R,C} w_{out} \tag{29}$$

$$COP_C = \frac{q_L}{q_{in}} = \eta_{th,C} COP_{R,c} = \left(1 - \frac{T_{ambient}}{T_{source}}\right)\left(\frac{T_{space}}{T_{ambient} - T_{space}}\right) \tag{30}$$

where $\eta_{th,c}$ is the thermal efficiency of the Carnot heat engine, $COP_{R,C}$ is the COP of Carnot refrigerator, and $T_{ambient}$, T_{space} and T_{source} are the ambient, space, and the heat source temperatures, respectively. For the proposed system the COP_C can be rewritten as (Kanoğlu et al. 2007):

$$COP_C = \left(1 - \frac{T_0}{T_8}\right)\left(\frac{T_5}{T_0 - T_5}\right) \tag{31}$$

The upper limit for any heat-driven air cooling system is the Carnot COP (Eq. 30). The open cycle desiccant air cooling system in both DER and DEV modes involves the mass transfer with the ambient and room. Water is added to the process air in the evaporative cooler, and humidity is increased in the room by the supplied channel. All of the added water is evaporated and returned to the ambient again. In this study, based on the method of (Lavan et al. 1982), equivalent Carnot temperatures for the evaporator, condenser, and heat source are employed. So, the reversible COP for open-cycle desiccant is calculated by (Lavan et al. 1982):

$$COP_{rev} = \left(1 - \frac{T_c}{T_s}\right)\left(\frac{T_e}{T_c - T_e}\right) \tag{32}$$

The abovementioned equivalent temperatures are heat source, evaporator, and condenser temperatures that are denoted by T_s, T_e, and T_c, respectively. These temperatures can be presented as follows (Kanoğlu et al. 2004):

$$T_s = \frac{h_7 - h_8}{s_7 - s_8} \tag{33}$$

$$T_e = \frac{\dot{m}_a h_4 - \dot{m}_a h_5 + \dot{m}_{w3} h_w}{\dot{m}_a s_4 - \dot{m}_a s_5 + \dot{m}_{w3} s_w} \tag{34}$$

$$T_c = \frac{\dot{m}_a h_9 - \dot{m}_a h_1 + (\dot{m}_{w1} + \dot{m}_{w2} + \dot{m}_{w3}) h_w}{\dot{m}_a s_9 - \dot{m}_a s_1 + (\dot{m}_{w1} + \dot{m}_{w2} + \dot{m}_{w3}) s_w} \tag{35}$$

where $\dot{m}_{w3}$ denotes the moisture rate that is added to supplied air in the room. Also, h_w and s_w indicate the liquid water enthalpy and entropy, respectively. It can be clearly pointed out that the reversible COP is a function of operating conditions. The exergy efficiency of the proposed desiccant system can be defined as follows (Song and Sobhani 2020):

$$\eta_{II,DCS} = \frac{\dot{E}_{cooling}}{\dot{E}_{reg}} \tag{36}$$

where $\dot{E}_{cooling}$ shows the exergy of cooling and $\dot{E}_{reg}$ is the regeneration exergy rate. These two expressions can be evaluated as follows (Song and Sobhani 2020):

$$\dot{E}_{cooling} = \dot{Q}_{cooling} \left|1 - T_a / T_{ave}\right| \tag{37}$$

$$\dot{E}_{reg} = \dot{m}_a \left[h_8 - h_7 - T_1 \left(s_8 - s_7\right)\right] \tag{38}$$

where T_a is the ambient temperature and T_{ave} denotes the average air temperature between room and supplied air. Also, the relation of entropy generation is as follows (Kanoğlu et al. 2004):

$$\dot{S}_{gen} = \sum \dot{m}_e s_e - \sum \dot{m}_i s_i - \sum \frac{\dot{Q}_k}{T_k} \tag{39}$$

Besides, the exergy destruction rate based on entropy generation can be obtained by use of Gouy–Stodola theorem (Kanoğlu et al. 2004):

$$\dot{E}_{lost} = T_0 \dot{S}_{gen} \tag{40}$$

Thus, the exergy destruction rate in different components of cooling system is defined by:

$$\dot{E}_{lost,DW} = T_0 \dot{m}_a \left(s_2 + s_9 - s_1 - s_8\right) \tag{41}$$

$$\dot{E}_{lost,HE} = T_0 \dot{m}_a \left(s_3 + s_7 - s_2 - s_6\right) \tag{42}$$

$$\dot{E}_{lost,EC1} = T_0 \left(\dot{m}_a s_4 - \dot{m}_a s_3 - \dot{m}_{w1} s_w\right) \tag{43}$$

$$\dot{E}_{lost,EC2} = T_0 \left(\dot{m}_a s_6 - \dot{m}_a s_5 - \dot{m}_{w2} s_w\right) \tag{44}$$

$$\dot{E}_{lost,reg} = T_0 \left(\dot{m}_a s_8 - \dot{m}_a s_7 - \frac{\dot{Q}_{reg}}{T_8}\right) \tag{45}$$

The exergy destruction for the whole desiccant system can be written as follows:

$$\dot{E}_{lost,Total} = \sum \dot{E}_{lost,Component} \tag{46}$$

For the AHU unit, the second law efficiency is calculated based on the required thermal energy of the building ($\dot{Q}_{AHU}$), the received thermal energy from the geothermal resource ($\dot{Q}_{Source}$), and total exergy destruction of the proposed system ($\dot{E}_{lost,Total}$). Thus;

$$\eta_{II,AHU} = \frac{\dot{Q}_{AHU}}{\dot{Q}_{Source} + \dot{E}_{lost,Total}} \tag{47}$$

Also, the total exergy efficiency of the proposed system can be calculated as:

$$\eta_{II,total} = \frac{\dot{Q}_{cooling} + \dot{Q}_{Heating}}{\dot{Q}_{Source} + \dot{E}_{lost,Total}} \tag{48}$$

Results and discussion

Model validation

In order to confirm the validity of the mathematical model and the obtained results for the proposed desiccant air conditioning system, the results of current study are compared with the data presented by (Kanoğlu et al. 2004). As depicted in Table 3, results match well with those reported by (Kanoğlu et al. 2004). It shows that the modeling is accurate enough to evaluate the proposed desiccant air cooling system.

The thermosiphon thermal resistance in the present study is validated with the presented data by (Perdikaris et al. 2009). As it can be observed in Table 4, excellent accuracy is obtained for the modeling of thermosiphon.

Parametric study

The parametric analysis investigates the effect of the various operating parameters on the efficiency of the system. The appropriate parameters, such as the temperature of regeneration air, the mass flow rate of the supplied air, humidity ratio, and ambient temperature, can be considered. In the present study, the humidity ratio of ambient air and temperatures of the ambient and regeneration line are considered as design parameters. The mass flow rate of the supplied and regeneration channel is introduced as the control parameters. As mentioned earlier, for the DEV system, the ambient air before entering into the evaporative cooler is mixed with the building conditioned air. For the DER system, the ambient air before entering into the desiccant wheel is mixed with the building conditioned air. The states of the proposed cycle are derived based on the cooling and heating loads of the office building; so, all of the system components provide the building required energy.

Table 3 Validation of the proposed desiccant air cooling system

States	P (kPa)	T (°C)	T_{wb}(°C)	$T_{wb,ref}$(°C)	ω(kgwater/kgdryair)	ω_{ref}(kgwater/kgdryair)	*RH*	RH_{ref}	h(kJ/kgdryair)	h_{ref}(kJ/kgdryair)	*s*(kJ/kgdryair)	s_{ref}(kJ/kgdryair)
1	101.3	31.5	19.69	19.70	0.009448	0.00950	0.329	0.329	55.98	56.01	5.795	5.803
2	101.3	43.5	21.01	21.00	0.006332	0.00630	0.115	0.115	60.03	60.00	5.815	5.813
3	101.3	30.2	16.72	16.70	0.006332	0.00630	0.2377	0.237	46.50	46.48	5.772	5.769
4	101.3	17.35	16.72	16.70	0.01165	0.01162	0.94	0.94	46.91	46.85	5.776	5.772
5	101.3	26.7	19.83	19.80	0.01165	0.01162	0.53	0.53	56.58	56.50	5.81	5.805
6	101.3	20.4	19.83	19.80	0.0143	0.01427	0.95	0.95	56.75	56.72	5.812	5.806
7	101.3	33.7	23.69	23.70	0.0143	0.01427	0.4349	0.435	70.45	70.43	5.855	5.852
8	101.3	60.8	30.09	30.10	0.0143	0.01427	0.11	0.11	98.44	98.41	5.945	5.940
9	101.3	49.8	29.4	29.40	0.01752	0.01747	0.227	0.227	95.45	95.39	5.937	5.933

Table 4 The validation of the thermosiphon model

Thermal resistances (K/kW)	R_1	R_2	R_3	R_4	R_5	R_6	R_7	R_8	R_9	R_{total}
Present model	17.68	1.075	0.165	1.56×10^{-05}	0	1.56×10^{-05}	0.165	1.075	17.68	37.85
(Perdikaris et al. 2009)	17.69	1.075	0.165	1.56×10^{-05}	0	1.56×10^{-05}	0.165	1.075	17.69	37.87

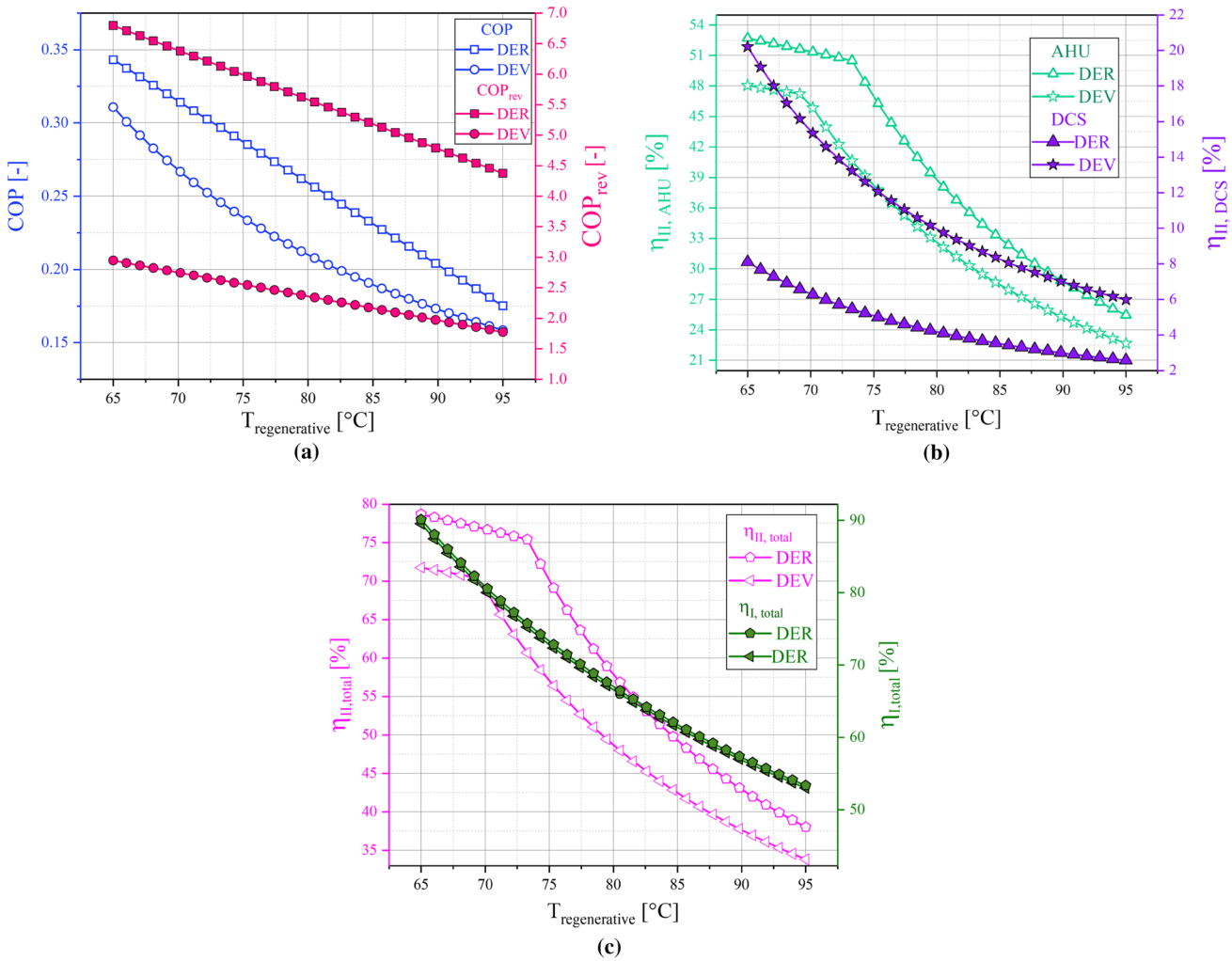

Fig. 4 The effect of the regeneration air temperature on the **a** COP and reversible COP of the desiccant air cooling systems, **b** Exergy efficiency of the DCS and AHU systems, **c** Energy and exergy efficiency of the proposed systems

Effect of the regeneration air temperature

The effect of the regeneration air temperature on the system performance is illustrated in Fig. 4. The reversible COP and total COP of the desiccant air cooling system are demonstrated in Fig. 4a. As shown, when the regeneration temperature changes between 65°C, and 95°C, both COP and COP_{rev} decrease. This is because of the increasing desiccant system thermal requirement with the increment of the regeneration temperature while the building cooling load is constant. Besides, both COP and COP_{rev} in DER scenario are higher than those of the DEV cycle. The second low-efficiency variations for the desiccant air cooling system and the AHU system in DER and DEV cycles are plotted in Fig. 4b. Based on the obtained results, it can be pointed out that the exergy efficiency for both DCS and AHU systems is decreased with the increment of the regeneration air temperature. Also, the values of the exergy efficiency of the desiccant unit for the DEV cycle is less than those of the DER cycle, and exergy efficiency for AHU indicates that the DEV cycle has good performance compared with the DER cycle in the considered interval for the regeneration temperature. Figure 4c shows

the proposed system total performance based on the energy and exergy analysis. According to this figure, with the increment of the regeneration temperature, the energy and exergy efficiencies of the DER and DEV cycles decrease. The thermal requirement of the regeneration channel is increased, which decreases the energy and exergy performance metrics of the total system.

Effect of the ambient air temperature

The ambient air plays the main role in the proposed system performance due to its impact on the building cooling load and desiccant air cooling system. The variation of the proposed system efficiency with the change in ambient air is plotted in Fig. 5. The variations of reversible COP and total COP of desiccant air cooling system are presented in Fig. 5a. According to this figure, for the DEV and DER systems, the total COP and COP_{rev} of DCS system are decreased with the increment of the ambient temperature. This is due to the increment of the building cooling load with the increment of ambient air temperature. Besides, the DER system efficiency in all ambient air temperatures is higher than that of the DEV system. The exergy efficiency changes of the DCS and AHU systems with the increment of the ambient air temperature are shown in Fig. 5b. As shown, both system exergy efficiency is decreased with the increment of the ambient air temperature. In fact, with the increment of $T_{ambient}$, the building requirements for cooling are increased and for the heating are decreased. In other words, increasing the cooling load requirements increases the regeneration channel thermal demands; this factor decreases the exergy efficiency. Also, the exergy efficiency in the DCS system for the DEV

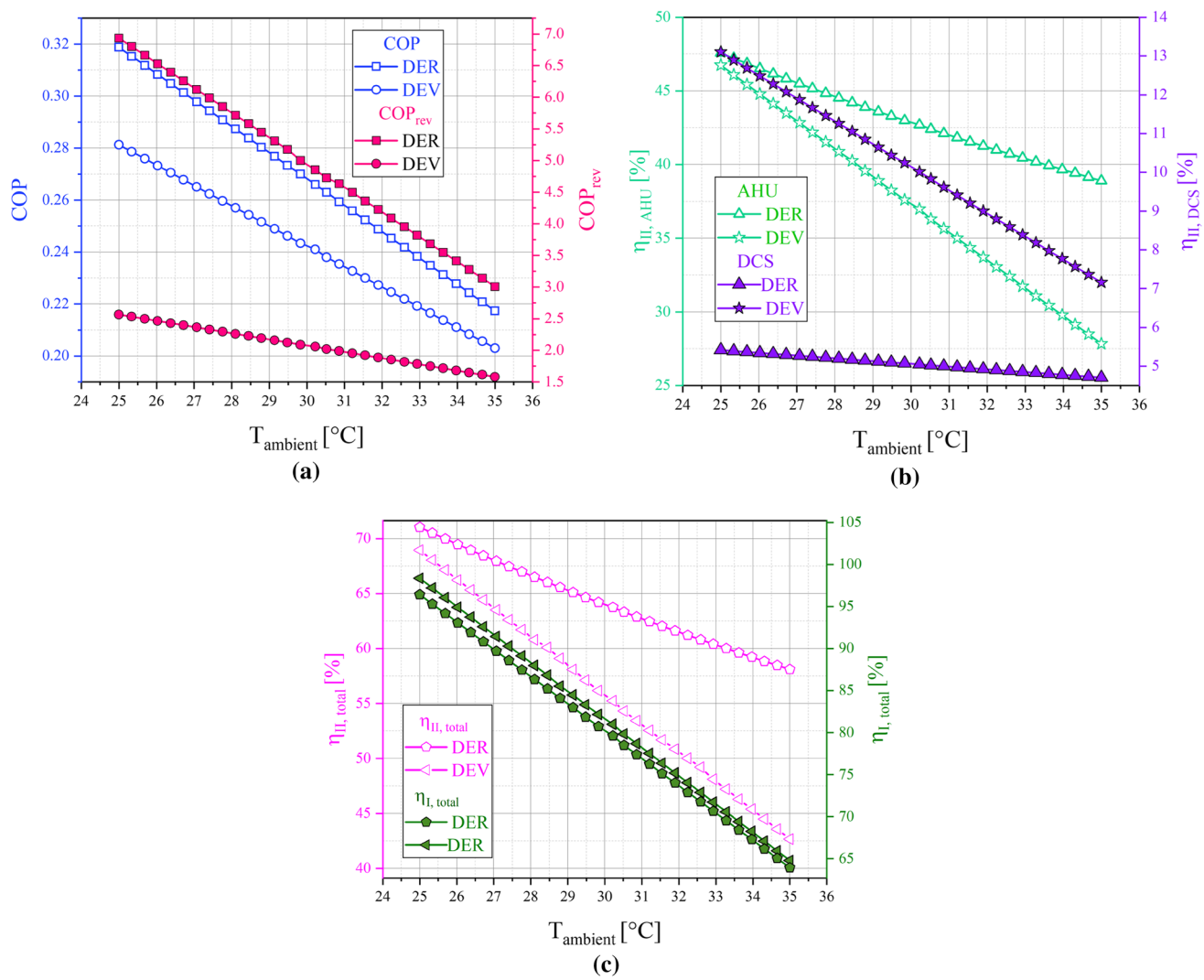

Fig. 5 The effect of the ambient air temperature on the **a** COP and reversible COP of the desiccant air cooling systems, **b** Exergy efficiency of the DCS and AHU systems, **c** Energy and exergy efficiency of the proposed systems

configuration is better than that of the DER system, and this efficiency for the AHU system is vice versa. Figure 5c illustrates the energy and exergy efficiencies of the proposed system. According to this figure, increasing the ambient air temperature decreases both energy and exergy efficiencies.

Effect of the humidity ratio of ambient air

To evaluate the impact of the air humidity ratio, it varied from 0.005kgwater/kgdryair to 0.035kgwater/kgdryair. The results are exhibited in Fig. 6a–c. Based on the results, considerable decreases in the performance metrics are observed with the increase in the air humidity ratio. For desiccant systems COP and COP_{rev}, the DER cycle shows better performance compared with the DEV cycle. In addition, for the desiccant air cooling system and AHU exergy efficiencies, the DEV and DER configurations indicate higher efficiencies, respectively. In evaluating the proposed system efficiency, the energy and exergy efficiencies for the DER system are better than the DEV configuration.

Effect of the air mass flow rate

The effect of air mass flow rate on the performance metrics is shown in Fig. 7. The air mass flow rate is assumed to be equal in both upper and lower channels of the DSC system. This parameter varied from 3000kg.h^{-1} to 9000kg.h^{-1}. As the air mass flow rate increases, the performance of the air to air heat exchanger (process 7 → 8) deteriorates and thermal requirements increases, so the system performance metrics decrease.

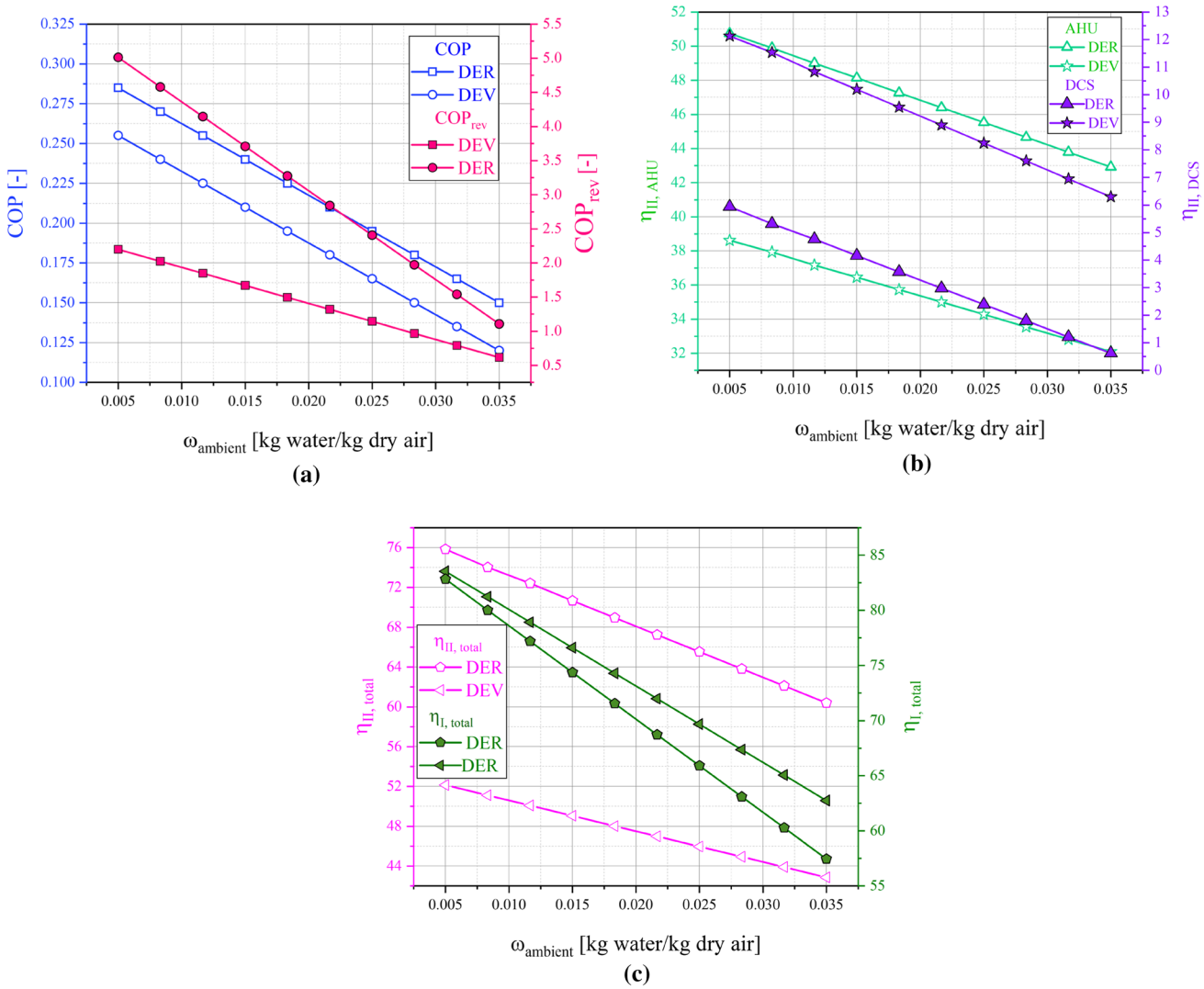

Fig. 6 The effect of the air humidity ratio on the **a** COP and reversible COP of the desiccant air cooling systems, **b** Exergy efficiency of the DCS and AHU systems, **c** Energy and exergy efficiency of the proposed system

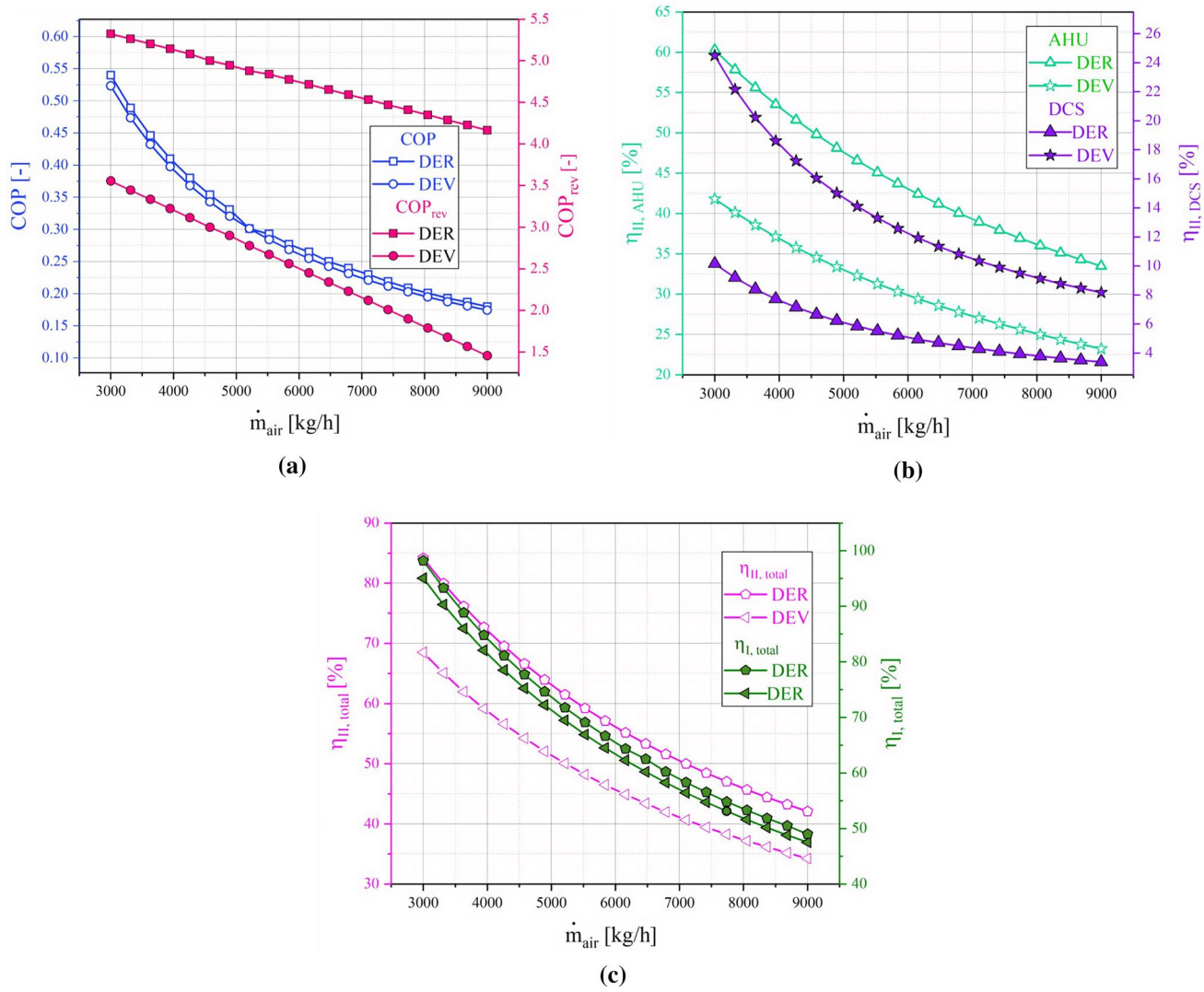

Fig. 7 The effect air mass flow rate on the **a** COP and reversible COP of the desiccant air cooling systems, **b** Exergy efficiency of the DCS and AHU systems, **c** Energy and exergy efficiency of the proposed system

The COP and COP_{rev} decrease with the increment of the air mass flow rate. This trend is repeated for the exergy efficiency of the DCS and AHU systems and the entire system energy and exergy efficiencies.

Main results of the modeling at the base case conditions

It is worthy to mention that based on the report of the Iranian National Building Regulations Office, the assumed ambient condition for summer and winter is presented in Table 5. The proposed system total behavior based on the intended space conditions for changes in humidity ratio, relative humidity, wet bulb temperature, and enthalpy of air at various state points for DER and DEV configurations is tabulated in Table 6.

Table 5 Weather conditions of Sarein city, in Ardabil, Iran

	T_{db}(°C)	T_{wb}(°C)	Daily changes (°C)	RH (%)	T_{DP}(°C)
Summer	29.7	20.26	1.6	52	16.3
Winter	21.9	–	–	78	–

The obtained data for supplied and regeneration channels and the AHU system is evaluated in the base case condition. Besides, due to the proposed cooling system

Table 6 Thermodynamic state properties for DER and DEV configurations

State	Fluid	P(kPa)	T_{db}(°C)	DER				DEV			
				RH	T_{wb}(°C)	ω (kgwater/kgdryair)	h (kJ/kgdryair)	RH	T_{wb}(°C)	ω (kgwater/kgdryair)	h (kJ/kgdryair)
0	Air	101.3	29.7	0.443	20.68	0.01156	59.45	0.443	20.68	0.01156	59.45
1	Air	101.3	29	0.443	20.52	0.01143	58.9	0.443	20.52	0.01143	58.9
2	Air	101.3	43.5	0.115	21.01	0.006332	60.14	0.115	21.01	0.006332	60.14
3	Air	101.3	30.2	0.2377	16.72	0.006332	46.59	0.2377	16.72	0.006332	46.59
4	Air	101.3	17.35	0.94	16.72	0.01165	46.96	0.94	16.72	0.01165	46.96
5	Air	101.3	25.6	0.4715	15.37	0.007976	46.09	0.4715	15.37	0.007976	46.09
6	Air	101.3	19.55	0.95	18.99	0.01356	54.07	0.95	18.99	0.01356	54.07
7	Air	101.3	33.7	0.4127	23.21	0.01356	68.67	0.4127	23.21	0.01356	68.67
8	Air	101.3	73.46	0.05974	32.24	0.01356	109.7	0.05974	32.24	0.01356	109.7
9	Air	101.3	49.8	0.227	29.4	0.01752	95.58	0.227	29.4	0.01752	95.58
10	Air	101.3	74.2	0.0579	32.38	0.01356	110.5	0.0579	32.38	0.01356	110.5
11	Geofluid	3.169	25	–	–	–	104.8	–	–	–	104.8
12	Geofluid	47.37	85	–	–	–	334.9	–	–	–	334.9
13	Geofluid	47.37	80	–	–	–	2643	–	–	–	2643
14	Geofluid	45.86	79.2	–	–	–	2642	–	–	–	2642
15	Geofluid	32.94	71.28	–	–	–	2628	–	–	–	2628
16	Geofluid	16.74	56.28	–	–	–	235.6	–	–	–	235.6
17	Air	101.3	70.49	–	–	–	106.7	–	–	–	106.7
18	Water	152	66.28	–	–	–	277.5	–	–	–	277.5
19	Water	152	19.5	–	–	–	81.88	–	–	–	81.88

importance, the psychrometric charts of the DER and DEV systems are illustrated in Fig. 8a and b, respectively. It is found that the humidity ratio of the supplied air is considerably decreased when passing through the desiccant wheel in the special regeneration air that is adjusted based on the ambient condition and building cooling load. The supplied air temperature is close to the designed room supply temperature by passing through the rotary regenerator and later through the evaporative cooler unit. The desiccant dehumidifier wheel provides the latent heat load of the DCS system.

Table 7 shows the effectiveness of components, the exergy efficiency of proposed cycles for DER and DEV systems. The desiccant wheel 2 has the lowest effectiveness (9.7%), and evaporative cooler 1 has the highest effectiveness, about 95.3% for the DER system. Also, the effectivenesses of the desiccant wheels in DER mode are low. As it can be seen from Table 7, the efficiency of the third desiccant wheel for the DER configuration is lower than that of the DEV system which means poor dehumidification performance. The exergy efficiencies for DER configuration in the heating and cooling system are about 50.2% and 5.42%, respectively, and these values for the DEV system are about 34.8% and 11.6%. A comprehensive comparison shows that the DER system has a better performance compared with the DEV system.

As mentioned earlier, the proposed system is designed according to the building cooling and heating loads. The thermal COP for the DER and DEV configurations is about 0.27 and 0.224. Also, the reversible COP for DER and DEV systems, are about 4.98 and 2.08, respectively. Based on this analysis, the radius of the thermosiphon pipe is evaluated about 0.02336m and 0.0221m for DER and DEV systems, respectively. Besides, the share of exergy destruction of each component and total exergy destruction of DER and DEV systems are given in Fig. 9. According to this figure, the exergy destruction of the DER system is less than the DEV configuration. The highest exergy destruction value belongs to the desiccant wheel, with 10.62kW and 10.02kW for DEV and DER configurations, respectively. Also, the lowest irreversibility is associated with evaporative cooler 2 for the DER system with about 0.53kW.

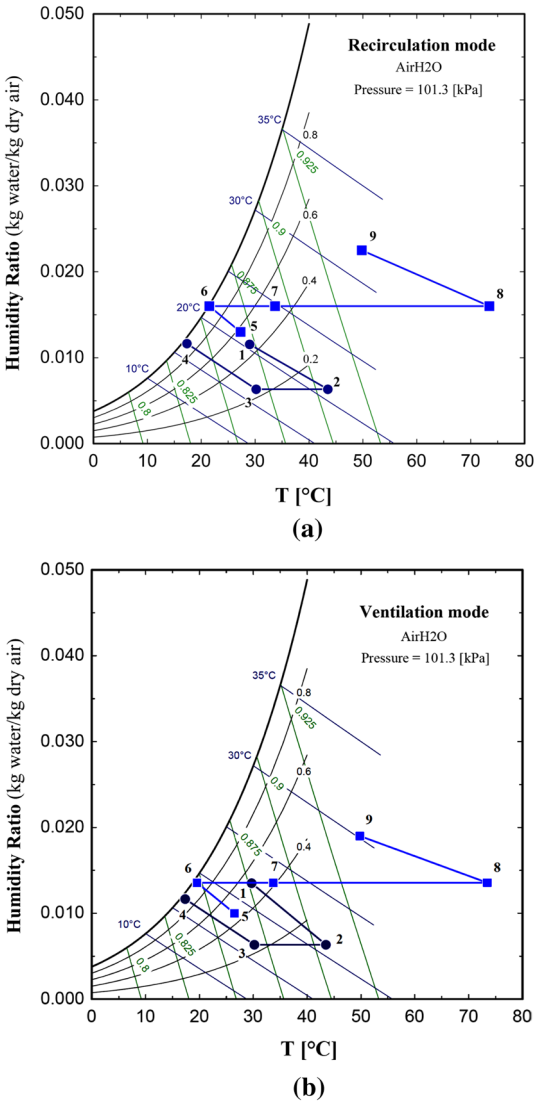

Fig. 8 Psychrometric charts **a** DER cycle **b** DEV cycle

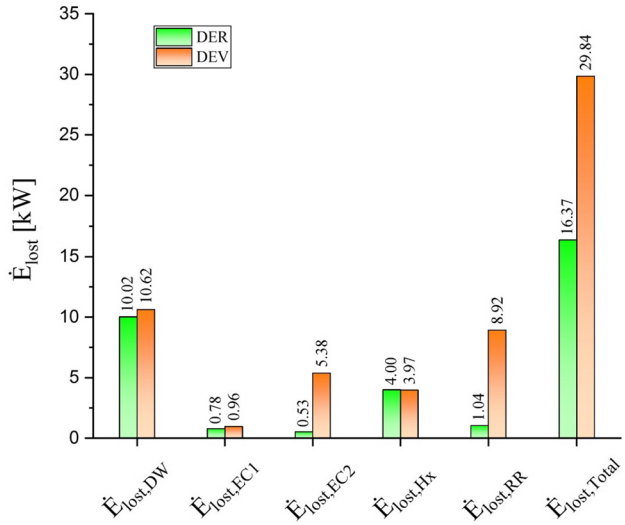

Fig. 9 Contribution of components exergy destruction of desiccant air cooling system for DER and DEV configurations

Table 7 Performance metrics of different components in the proposed cycle

Parameter	Cycle	
	DER	DEV
T_{reg}(°C)	73.4	73.4
ε_{EC1}(%)	95.3	95.3
ε_{EC2}(%)	91.7	59.16
ε_{RR}(%)	57.5	55.5
ε_{Dw1}(%)	37.4	31.8
ε_{Dw2}(%)	9.7	32
ε_{Dw3}(%)	20.6	44.5
$\eta_{II,DCS}$(%)	5.42	11.6
$\eta_{II,AHU}$(%)	50.2	34.8
$\eta_{I,cycle}$(%)	81.75	81.8
$\eta_{II,cycle}$(%)	75.0	52

Conclusion

The use of low-grade geothermal energy sources in the different thermal-activated systems and direct uses is more efficient. In the present paper, the geothermal energy has been extracted using the thermosiphon pipe from hot springs of inactive volcano mountain, Sabalan. The obtained geothermal energy has been divided in the cascade main heat exchanger to supply the cooling and heating loads of selected office building. The solid desiccant air conditioning system has been applied in two DER and DEV configurations for supplying the cooling load. In the DER system, the ambient air before entering into the desiccant wheel mixed with the building conditioned air. While, for the DEV system, the ambient air before entering into the evaporative cooler mixed with the building conditioned air. For the building heating requirements, the AHU system has been utilized that receives its heat from the low thermal level of the cascade heat exchanger. The proposed cycles with a new configuration have been thermodynamically analyzed to assess the system efficiency, and the parametric study has been conducted to enhance the system efficiency. The main findings of the presented paper can be summarized as follows:

The optimum diameter of the two-phase closed thermosiphon pipe has been calculated at about 0.02336m and 0.0221m for DER and DEV configurations based on the concept of the network thermal resistances as well as thermal demands of the assumed building.

The calculations have shown that the energy efficiency for the DER and DEV systems is about 81.75% and 81.8%, respectively.

The exergy efficiency for DER configuration in the heating and cooling system was about 50.2% and 5.42%, respectively, and these values for the DEV system were about 34.8% and 11.6%, respectively.

The exergy destructions of the DER system were less than the DEV configuration. The highest exergy destruction value belonged to the desiccant wheel, with 10.62 kW and 10.02 kW for DEV and DER configurations, respectively. It can be clearly pointed out that the use of geothermal energy, especially in the solid desiccant system, will lead to better performance of the system, environmental benefits, and improving indoor air quality.

Acknowledgements The authors wish to thank all who assisted in conducting this work.

Declarations

Conflict of interest The authors declare that they have no known competing financial interests or personal relationships that could have appeared to influence the work reported in this paper.

References

Ali A, Ishaque K, Lashin A, Al Arifi N (2017) Modeling of a liquid desiccant dehumidification system for close type greenhouse cultivation. Energy 118:578–589

Berardi U, Heidarinejad G, Rayegan S, Pasdarshahri H (2020) Enhancing the cooling potential of a solar-assisted desiccant cooling system by ground source free cooling, In: Building Simulation. Springer, pp. 1125–1144

Bourdoukan P, Wurtz E, Joubert P (2009) Experimental investigation of a solar desiccant cooling installation. Sol Energy 83:2059–2073

Caliskan H, Hong H, Jang JK (2019) Thermodynamic assessments of the novel cascade air cooling system including solar heating and desiccant cooling units. Energy Convers Manag 199:112013

Cengel YA, Boles MA, Kanoglu M (2011) Thermodynamics: an engineering approach. McGraw-hill New York

Chang C-C, Liang J-D, Chen S-L (2018) Performance investigation of regenerative total heat exchanger with periodic flow. Appl Therm Eng 130:1319–1327

Chen Y, Yang H, Luo Y (2018) Investigation on solar assisted liquid desiccant dehumidifier and evaporative cooling system for fresh air treatment. Energy 143:114–127

Dunn P, Reay D (2016) Heat pipes. Elsevier, Amsterdam

Emhofer J, Beladi B, Dudzinski P, Fleckl T, Kuhlmann HC (2017) Analysis of a cross-flow liquid-desiccant falling-film. Appl Therm Eng 124:91–102

Fong KF, Lee CK (2020) Solar desiccant cooling system for hot and humid region–a new perspective and investigation. Sol Energy 195:677–684

Gómez-Castro FM, Schneider D, Päßler T, Eicker U (2018) Review of indirect and direct solar thermal regeneration for liquid desiccant systems. Renew Sustain Energy Rev 82:545–575

Hassanpour A, Borji M, Ziapour BM, Kazemi A (2020) Performance analysis of a cascade PCM heat exchanger and two-phase closed thermosiphon: a case study of geothermal district heating system. Sustain. Energy Technol. Assessments 40:100755

Heidari A, Roshandel R, Vakiloroaya V (2019) An innovative solar assisted desiccant-based evaporative cooling system for co-production of water and cooling in hot and humid climates. Energy Convers Manag 185:396–409

Kabeel AE (2010) Dehumidification and humidification process of desiccant solution by air injection. Energy 35:5192–5201

Kabeel AE, Khalil A, Elsayed SS, Alatyar AM (2018a) Theoretical investigation on energy storage characteristics of a solar liquid desiccant air conditioning system in Egypt. Energy 158:164–180

Kabeel AE, Khalil A, Elsayed SS, Alatyar AM (2018b) Dynamic behaviour simulation of a liquid desiccant dehumidification system. Energy 144:456–471

Kanoğlu M, Çarpınlıoğlu MÖ, Yıldırım M (2004) Energy and exergy analyses of an experimental open-cycle desiccant cooling system. Appl Therm Eng 24:919–932

Kanoğlu M, Bolattürk A, Altuntop N (2007) Effect of ambient conditions on the first and second law performance of an open desiccant cooling process. Renew Energy 32:931–946

Lavan Z, Monnier J-B, Worek WM (1982) Second law analysis of desiccant cooling systems

Liang J-D, Hsu C-Y, Hung T-C, Chiang Y-C, Chen S-L (2018) Geometrical parameters analysis of improved circulating inclined fluidized beds for general HVAC duct systems. Appl Energy 230:784–793

Liang J-D, Huang B-H, Chiang Y-C, Chen S-L (2020) Experimental investigation of a liquid desiccant dehumidification system integrated with shallow geothermal energy. Energy 191:116452

Mills AF (1995) Heat and mass transfer. Richard D. Irwin, Chicago

Mohammad AT, Mat SB, Sulaiman MY, Sopian K, Al-abidi AA (2013) Historical review of liquid desiccant evaporation cooling technology. Energy Build 67:22–33

Mojaver P, Khalilarya S, Chitsaz A (2018) Performance assessment of a combined heat and power system: a novel integrated biomass gasification, solid oxide fuel cell and high-temperature sodium heat pipe system part I: Thermodynamic analysis. Energy Convers Manag 171:287–297

Nada SA (2017) Air cooling-dehumidification/desiccant regeneration processes by a falling liquid desiccant film on finned-tubes for different flow arrangements. Int J Therm Sci 113:10–19

Park J-Y, Yoon D-S, Lee S-J, Jeong J-W (2016) Empirical model for predicting the dehumidification effectiveness of a liquid desiccant system. Energy Build 126:447–454

Perdikaris N, Panopoulos KD, Fryda L, Kakaras E (2009) Design and optimization of carbon-free power generation based on coal hydrogasification integrated with SOFC. Fuel 88:1365–1375

Rayegan S, Motaghian S, Heidarinejad G, Pasdarshahri H, Ahmadi P, Rosen MA (2020) Dynamic simulation and multi-objective optimization of a solar-assisted desiccant cooling system integrated with ground source renewable energy. Appl Therm Eng 173:115210

Rosiek S, Batlles FJ (2012) Shallow geothermal energy applied to a solar-assisted air-conditioning system in southern Spain: two-year experience. Appl Energy 100:267–276

Song J, Sobhani B (2020) Energy and exergy performance of an integrated desiccant cooling system with photovoltaic/thermal using phase change material and maisotsenko cooler. J Energy Storage 32:101698

Speerforck A, Schmitz G (2016) Experimental investigation of a ground-coupled desiccant assisted air conditioning system. Appl Energy 181:575–585

Speerforck A, Ling J, Aute V, Radermacher R, Schmitz G (2017) Modeling and simulation of a desiccant assisted solar and geothermal air conditioning system. Energy 141:2321–2336

Thu K, Mitra S, Saha BB, Murthy SS (2018) Thermodynamic feasibility evaluation of hybrid dehumidification–mechanical vapour compression systems. Appl Energy 213:31–44

Wang X, Zhu Y, Zhu M, Zhu Y, Fan H, Wang Y (2017) Thermal analysis and optimization of an ice and snow melting system using geothermy by super-long flexible heat pipes. Appl Therm Eng 112:1353–1363

Wang X, Liu H, Wang Y, Zhu Y (2020) CFD simulation of dynamic heat transfer behaviors in super-long thermosyphons for shallow geothermal application. Appl Therm Eng 174:115295

William GE, Mohamed MH, Fatouh M (2015) Desiccant system for water production from humid air using solar energy. Energy 90:1707–1720

Xie Y, Zhang T, Liu X (2016) Performance investigation of a counterflow heat pump driven liquid desiccant dehumidification system. Energy 115:446–457

Yang Z, Zhang K, Yang M, Lian Z (2014) Improvement of the ultrasonic atomization liquid desiccant dehumidification system. Energy Build 85:145–154

Yang Z, Lin B, Zhang K, Lian Z (2015) Experimental study on mass transfer performances of the ultrasonic atomization liquid desiccant dehumidification system. Energy Build 93:126–136

Yinglin L, Xiaosong Z, Laizai T, Zhongbin Z, Wei W, Xueying X (2016) Performance analysis of a novel liquid desiccant-vapor compression hybrid air-conditioning system. Energy 109:180–189

Yousefi H, Noorollahi Y, Ehara S, Itoi R, Yousefi A, Fujimitsu Y, Nishijima J, Sasaki K (2010) Developing the geothermal resources map of Iran. Geothermics 39:140–151

Zorn R, Steger H, Kolbel T, (2015) De-icing and snow melting system with innovative heat pipe technology, In: Proceedings World Geothermal Congress, Melbourne, Australia. pp. 19–25